Linear optical properties and electronic structures of poly(3-hexylthiophene) and poly(3-hexylselenophene) crystals from first principles

Takao Tsumuraya,* Jung-Hwan Song,† and Arthur J. Freeman
Department of Physics and Astronomy, Northwestern University, 2145 Sheridan Road, Evanston, Illinois, 60208-3112, USA
(Received 18 April 2012; published 8 August 2012)

Linear optical properties of regio-regular-poly(3-hexythiophene) (rr-P3HT) and regio-regular-poly(3-hexyselenophene) (rr-P3HS) are investigated in relation to their anisotropic crystal structure by means of first-principles density functional calculations. The optical spectra are evaluated by calculating its dielectric functions, focusing on the frequency dependence of the imaginary part. The optical transition along the π conjugation-connecting backbone direction is found to be the most significant at the band edges. A group-theoretical analysis of the matrix elements is given to explain the interband transitions. The optical spectra, electronic structures, and structural stabilities are calculated using the all-electron full-potential linearized augmented plane wave (FLAPW) method within the local-density approximation. We proposed several possible crystal structures of rr-P3HT and performed structural optimizations to determine a stable structure. Comparing the total energy differences among these relaxed structures, a base-centered monoclinic structure belonging to the space group $A2$ is found to be the most stable structure. In the electronic structure, C and S orbitals belonging to polythiophene backbones are the biggest contributors at the valence band maximum and conduction band minimum, but there is almost no contribution from the hexyl side chains. Last, the differences in electronic and optical properties between rr-P3HT and rr-P3HS are discussed.

DOI: 10.1103/PhysRevB.86.075114 PACS number(s): 71.20.−b, 71.15.Mb, 72.80.Le, 78.20.−e

I. INTRODUCTION

Semiconducting polymers have attracted great interest as electron donor materials in bulk-heterojunction (BHJ) photovoltaics[1–4] and charge transport materials in polymer-based field-effect transistors (PFETs).[5–8] These organic electronic devices are promising alternatives to traditional silicon-based devices because of their relatively large area, low-cost fabrication, and mechanically flexible substrates associated with polymers.[9] In this context, regio-regular-poly(3-hexythiophene) (rr-P3HT) is widely used in BHJ solar cells, since power conversion efficiency surpassing 5% has been achieved for the devices in direct contact with the fullerene derivative[6]-phenyl-C_{61}-butylic acid methylester ($PC_{61}BM$).[2,10] This material exhibits relatively high charge (electron/hole) mobilities (up to 10^{-2}–10^{-1} $cm^2/V{\cdot}s$.), which is comparable to that of amorphous silicon.[11] In these applications, the performance of devices is strongly dependent on the thin-film structure and morphology of the donor polymer on substrates.[12,13]

Rr-P3HT is one of the family of regio-regular-poly(3-alkylthiophenes) (rr-P3ATs). Figure 1 shows the basic chemical structure of rr-P3AT. All polymers that belong to this family consist of rigid backbones called polythiophenes (PTs) with pendant alkyl side chains $[(CH_2)_{n-1}CH_3]$.[14] Regio-regular means that alkyl side chains on adjacent PT backbones are ordered in a "head to tail" conformation.[15,16] Semicrystalline polymers exhibit highly ordered crystalline regions with disordered amorphous regions.[17] In the family of P3ATs, two polymorphs, called Forms I and II, have been observed, which differ mainly by the side-chain conformations.[18–20] Structural determinations for the Forms I of rr-P3HT ($n = 6$) have been performed on the basis of x-ray/electron diffraction measurements.[21–26] Most papers published in the 1990s show only schematic models and lattice constants of crystal rr-P3AT; none are about internal coordinates and space groups.[18,21,22,27,28] In recent years, a monoclinic structure of rr-P3HT with a $P2_1/c$ space group was proposed by small-angle electron diffraction measurements.[20,29] To determine the stable crystal structure, several groups examined first-principles density functional theory (DFT) calculations and discussed their structural properties.[30–35] However, most of these studies have been carried out using tentative orthorhombic lattices. The possibility that the material shows space groups with lower symmetry and its optical properties have not yet been theoretically discussed.

More recently polyselenophenes such as regio-regular-poly(3-hexylselenophene) (rr-P3HS) and poly(3-octylselenophene) have attracted interest in analogy with polythiophenes because polyselenophenes have a slightly smaller measured optical band gap than polythiophenes.[36] Their chemical structure is almost the same as that of rr-P3HT, but the sulfur atoms in the backbones are substituted by selenium atoms. It has been expected that the narrower band gap of rr-P3HS may lead to a more pronounced absorption in the BHJ device.[37] However, no significant improvement of the performance has been reported from experiments.[38] Differences, in the optical properties and electronic structures due to the replacement have not been theoretically investigated as yet.

In the present study, we elucidate the structural-optical property relationships that govern the optical transitions of the conjugated polymers on the basis of first-principles DFT calculations. Possible crystal structures for the Form I of rr-P3HT are proposed, and the stable structure is determined by performing structural optimizations and total energy calculations, which can shed light on the experimental observation of various structures. Once the stable crystal structure of the polymer is known, its electronic band structure, density of states (DOS), and linear optical properties in terms of dielectric functions

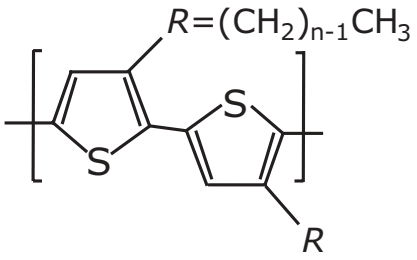

FIG. 1. Chemical structure of regio-regular-P3ATs.

are accurately calculated by the all-electron full-potential linearized augmented plane wave (FLAPW) method. The differences in the electronic structures and optical properties between rr-P3HT and rr-P3HS are also discussed.

II. COMPUTATIONAL DETAILS

Linear optical spectra and electronic structures are calculated using the all-electron FLAPW method[39–42] based on DFT.[43,44] The exchange and correlation energies are treated within the local density approximation (LDA) with the Hedin and Lundqvist form of exchange correlation functional.[45] Dielectric functions are calculated according to time-dependent perturbation theory using the electric dipole matrix elements based on the FLAPW method.[46,47] Here we focus on its imaginary part $\epsilon_2(\omega)$. The basic expression, in terms of the band structure and the dipole matrix elements of the perturbation due to the interaction with photons, is written as

$$\epsilon_2(\omega) = \frac{8\pi^2 e^2}{\omega^2 m^2 V} \sum_{i,f} \sum_{\mathrm{k}} |\langle \psi_{f,\mathbf{k}} | \hat{\mathbf{e}} \cdot \mathbf{p} | \psi_{i,\mathbf{k}} \rangle|^2 \delta_b \times [E_f(\mathbf{k}) - E_i(\mathbf{k}) - \hbar\omega], \quad (1)$$

where $\hat{\mathbf{e}}$ is the photon electric polarization vector, and $\mathbf{p}$ is the electric dipole operator. The sum is over the unit cell of volume V. The electric dipole matrix elements are calculated for the direct interband transition between the occupied $|\psi_{i,\mathbf{k}}\rangle$ and unoccupied $|\psi_{f,\mathbf{k}}\rangle$ states whose eigenenergies are E_i and E_f, respectively. The absorption coefficient μ is defined as

$$\mu = \frac{\epsilon_2 \omega}{nc}, \quad (2)$$

where $\epsilon_1 = n^2 - \kappa^2$ and $\epsilon_2 = 2n\kappa$. μ gives the rate of spatial decay and has units of inverse length. The real part of the dielectric function ϵ_1 can be obtained from ϵ_2 by the Kramers-Kronig integral transformation.[48]

Structural optimizations for all lattice constants, angles, and internal atomic coordinates were performed based on the following procedure: The Vienna *ab initio* simulation program[49,50] with projected augmented wave potentials was used for relaxing lattice shapes by calculating stress tensor; an energy cutoff of 800 eV was used for the plane wave basis functions. We confirmed that the relaxed structural parameters based on the pseudo-potential method are in fairly good agreement with those based on the FLAPW method. The structural stabilities, electronic structures, and optical properties are calculated using the FLAPW methods. Uniform k-mesh sets of $4 \times 6 \times 6$ for the $A2$ structures,$4 \times 6 \times 10$ for the $P2_1$, and $2 \times 6 \times 6$ for the $P2_1/a$ structure were used in the Brillouin zone integrations. Muffin-tin sphere radii were set to be 1.03 Å for S, 0.68 Å for C, and 0.40 Å for H, respectivity. The plane-wave cutoffs were set to 30 Ry for the LAPW basis functions, and the cutoffs of the potential representation were set to 135 Ry. We have checked the convergence of total energies, in terms of the plane-wave cutoffs for the basis functions and the electron densities.

III. RESULTS AND DISCUSSION

A. Determination of crystal structure of rr-P3HT

The crystal structures of rr-P3HT have been extensively investigated using various experimental techniques. Table I shows experimentally proposed lattice parameters. The results, most from papers published in the 1990s, show only schematic models and lattice constants of crystal rr-P3AT; none are about internal coordinates and space groups. Prosa *et al*. reported a structural model, called the inverse comb model, that has lamellar structures by which stacks of PT backbones are found to be uniformly spaced by the side chains.[18,27,28] Tashiro *et al*. proposed various possible schematic models of rr-P3HT using computational modeling techniques.[21,22] Quite recently a monoclinic structure of rr-P3HT with a $P2_1/c$ space group was proposed by the electron diffraction measurements.[20,29]

Here there are two uncertain points related to the structural type: Does crystalline rr-P3HT have an orthorhombic or monoclinic structure, and is the lattice constant a about 32 or 16 Å. Furthermore, no consensus on the internal coordinates has been obtained. Our proposed structures with their optimized lattice parameters and the energy differences (E_{total}) among them are summarized in Tables II and III, respectively. We found that a base-centered monoclinic structure, type β', is the most stable structure, but the energy difference between types β and β' is quite small. Details of the proposed

TABLE I. Experimentally determined lattice constants of rr-P3HT. XRD represents x-ray diffraction measurements. SAED shows small-area electron diffraction measurements.

Type	Method	Space group	a (Å)	b (Å)	c (Å)	β (°)
Prosa *et al*.[18,27]	XRD		33.60	7.7	7.66	90
Kawai *et al*.[61]	XRD		16.72	7.77	7.57	90
Tashiro *et al*.[21]	XRD		16.63	7.77	7.75	90
Tashiro *et al*.[22]	XRD		33.26	7.77	7.75	90
Kayunkid *et al*.[29]	SAED	$P2_1/a$	16.00	7.8	7.8	86.5

TABLE II. Relaxed lattice parameters for proposed structures of rr-P3HT compared with previous DFT studies. δ_b is an interplanar offset between upper and lower sheets. Optimized unit-cell volume V (Bohr^3).

This study	Approximation	Space group	a (Å)	b (Å)	c (Å)	β (°)	δ_b	V (a.u.)
α'	LDA	$A2_122$	34.12 (17.06)	7.73	6.89	90	0.5	3068.01
β	LDA	$A2$	16.90	7.71	7.55	92.03	0.5	3316.77
β'	LDA	$A2$	16.22	7.73	7.02	100.96	0.5	2918.20
γ'	LDA	$P2_1/a$	16.27	7.72	7.15	89.02	0.058	3026.42
κ'	LDA	$P2_1$	18.56	7.74	3.74 (7.48)	86.57	0	3618.54
Other DFT studies								
Maillard and Rochefort[32]	LDA		15.82	7.83	6.84	90	0.5	
Xie *et al.*[35] I(LL)	GGA + LAP		17.24	7.80	7.70	90	0	
Xie *et al.*[35] II(LL)	GGA + LAP		17.09	7.80	7.09	101	0.5	
Xie *et al.*[35] III(LR)	GGA + LAP		18.91	7.80	6.73	87	0.2	
Dag and Wang[33]	GGA + D		16.76	7.81	7.71	90	0.5	

structures, including results of their structural optimizations, are presented in following subsections.

As shown in Fig. 2, the lattice constants are defined following the notation given below. These reported structures share the following common structural features: lattice constant a corresponds to the length of the hexyl side-chain stacking direction (x axis), b is the (π conjugation) connecting backbone direction (y axis), and c exhibits the PT backbone (π-π) stacking direction (z axis). The extension of the side chains is essentially along the x axis in the P3AT family.[17] To characterize the molecular packing depending on the different structures, we need to focus on (1) orientations of the PT backbone and the hexyl side chains in the ac plane, (2) angular orientation of the plane containing the hexyl side chain with zig-zag conformation, and (3) interplanar offset between lower and upper molecular sheets along the conjugated direction, y axis, in the unit cell (δ_b).

1. *Base-centered orthorhombic ($A2_122$) and monoclinic ($A2$) structures*

We first proposed two possible crystal structures of rr-P3HT. One is a base-centered orthorhombic structure with $A2_122$ (No. 20) as shown in Fig. 3(a), and the other is a base-centered monoclinic structure with $A2$ space group (No. 4) as shown in Fig. 3(b). We refer to the orthorhombic structure as type α and the monoclinic one as β, respectively. Type α consists of 100 atoms/cell, and β contains 50 atoms/cell. The structural model of β is constructed by cutting half of the unit cell off from α structure. This indicates that the $A2_122$ structure consists of four monomeric units, and $A2$ contains two units in the conventional cell. Both structures have a twofold screw axis rotation around the y axis, which is orthogonal to the PT stacking axis.

As in the orthogonal views in Fig. 3(b), the PT backbones in the monoclinic $A2$ structure are stacked isodirectionally along the x axis, while those in the orthorhombic type α have an antiparallel configuration as a consequence of the space groups. As in the top views shown in Fig. 4, although both structures have a herringbone structure, the $A2$ structure exhibits a "parallel" lamellar structure, and the $A2_122$ structure shows a "zigzag" lamellar one. The atomic coordinates of type α are taken from a structural model of rr-poly(3-butilthiophene) (P3BT) ($n = 4$) proposed by Arosio *et al.*,[51] which was obtained on the basis of a Rietveld refinement of a powder diffraction pattern and molecular mechanics calculations, in analogy with poly(3-methylbutylthiphene) (P3MBT).[52] We extended the length of the side chains to be hexyl side chains since the structural difference between rr-P3HT and rr-P3BT might be simply due to the length of the side chains.

To compare the differences in stabilities between the two structures, we first constructed the crystal structures employing the experimentally determined lattice parameters observed by Tashiro *et al.*[21,22] The lattice constant a for the type α structure is set to be twice as large as that for type β, and the monoclinic angle β is set to be 90° for the comparison; lattice constants $b = 7.77$ Å and $c = 7.75$ Å are used for both structures. The relaxation for their internal coordinates was performed by the FLAPW method. As a result of the relaxation, we found that type β is more stable than type

TABLE III. Calculated total energy differences and band gaps of crystalline rr-P3HT.

Polymer	Type	Space group	E_{total} [eV/f.u.]	Indirect gap [eV]	Direct gap (Γ) [eV]
rr-P3HT	γ'	$P2_1/a$	1.32	0.86	0.84
	κ'	$P2_1$	0.37	0.75	1.01
	α'	$A2_122$	0.35	0.28	1.44
	β	$A2$	0.22	0.59	1.09
	β'	$A2$	0	0.38	1.01
rr-P3HS	β	$A2$		0.20	0.86

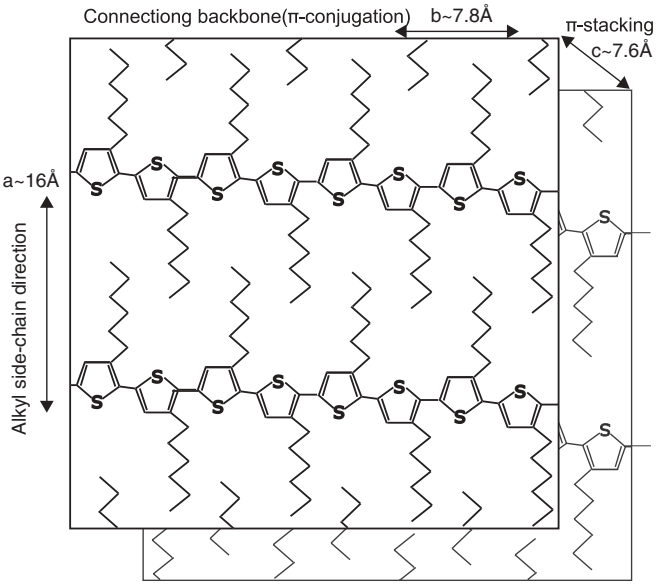

FIG. 2. Schematic diagram of crystal structures in rr-P3HT. The conjugation direction and the π-π stacking direction are fast charge transport directions.

α. The total energy difference is 0.22 eV/50 atoms. The tails of the side chains of neighboring molecules of the α structure are very close to one another, which leads to repulsive atomic forces between them. The β structure is monoclinic; we optimized the lattice volumes and monoclinic angle β around the experimental lattice volume. The relaxed lattice parameters are $a = 16.90$, $b = 7.71$, $c = 7.55$ Å, and $\beta = 87.97^\circ$, which are in fairly good agreement with the experimentally proposed lattice parameters. The calculated energy difference between β equal to 90° and 87.97° is 0.24 eV/50 atoms; this plays an important role in stabilizing the monoclinic structure.

Second, we performed full structural optimizations for both α and β structures using the pseudopotential method. Figure 3(c) and 3(d) show the fully relaxed structures called types α' and β', respectively. As a result of comparing between before and after the relaxation, two molecular units are separated from one another in type α' as opposed to the α structure. This can be seen in Fig. 3(c), which results in the lattice constant a in α' being longer than that of α. Furthermore, as a result of the full relaxation for the β structure, we found a more stable structure with the $A2$ space group, as shown in Fig. 3(d) (called type β'). The optimized lattice parameters of type β' are $a = 16.23$ Å, $b = 7.73$ Å, $c = 7.03$ Å, and $\beta = 101.24^\circ$. In this structure the neighboring two side chains are interjected into one another along the stacking direction of backbones (z).

In the present study, we found that the β' structure is the most energetically stable among proposed structures. However, the optimized interplanar distance between two PT backbones is about 3.50 Å, which is shorter than that 3.77 Å, obtained from experiment.[21] Furthermore, the calculated monoclinic angle β has not yet been reported by experiments. A previous theoretical study by Xie *et al.* also proposed similar structures with a monoclinic angle $\beta = 101^\circ$ by using a semiempirical (*ad hoc*) method based on the DFT + a local atomic potential (LAP) approach. This method partially takes the electronic nature of van der Waals (vdW) interactions into account; the interaction is represented by a local parameterized

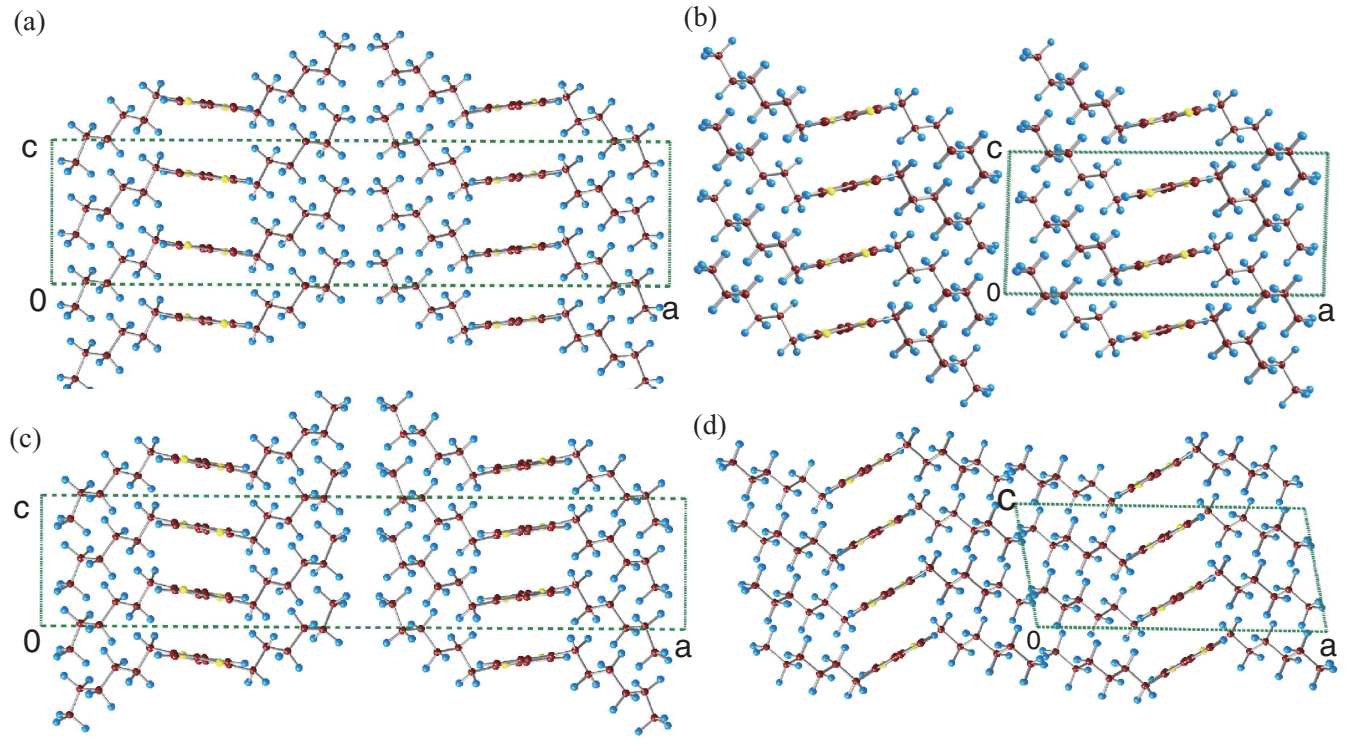

FIG. 3. (Color online) Orthogonal views of (a) α, (b) β, (c) α', and (d) β' structures along the b axis showing the ac plane. Yellow circles show sulfur atoms, red circles show carbon atoms, and blue circles show hydrogen atoms. Green dashed lines represent the conventional unit cell.

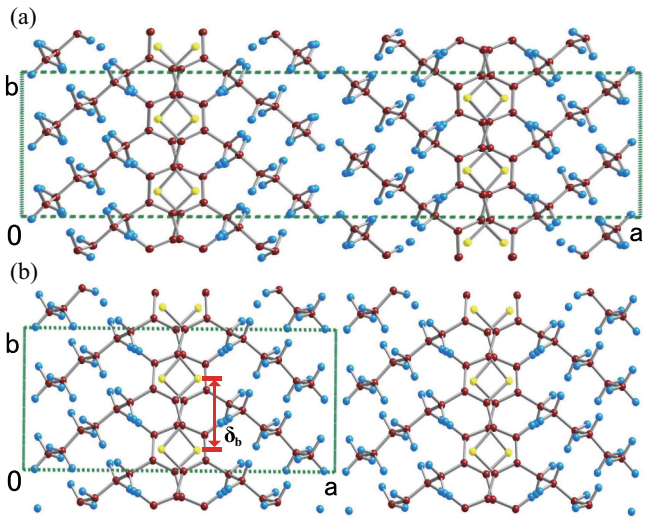

FIG. 4. (Color online) Longitudinal views of (a) α and (b) β' structures along the b axis showing the ac plane. Yellow circles show sulfur atoms, red circles show carbon atoms, and blue circles show hydrogen atoms. Green dashed lines represent conventional unit cell.

contribution added to atomic pseudopotentials. They found that their proposed structure with interplanar offset along the b axis, $\delta_b = b/2$, is stabilized at $\beta = 101^\circ$, while another structure with $\delta_b = 0$ is stabilized at $\beta = 90^\circ$. It is also noted that the offset value of the β' structure of $\delta_b = b/2$ is in generally good agreement with several structures of rr-P3HT proposed by previous DFT studies[32,33] and experiments, and other polythionene crystals such as PMBT[52] and poly(3,4-ethylenedioxythiophene) (PEDOT).[53,54]

2. *Monoclinic structure with $P2_1/c$*

Recently Kayunkid *et al.* synthesized semicrystalline samples of rr-P3HT epitaxial thin films and reported another monoclinic structure with $P2_1/c$ space group (No. 14) on the basis of electron diffraction measurements.[29] This lattice contains 100 atoms per unit cell where C, H, and S atoms occupy 4a Wyckoff sites. The axis choice of the unit cell can be transferred along with $P2_1/a$ or $P2_1/n$, depending on the axis choice of the unit cell. Their proposed lattice parameters with the $P2_1/a$ are $a = 16.0$ Å, $b = 7.80$ Å, $c = 7.80$ Å, and $\beta = 86.5^\circ$; we term this structure type γ. Figure 4(a) shows an orthogonal view of the monoclinic structure. There are several remarkable characteristics of type γ compared to α and β. One is that the zig-zag plane of the hexyl side chains in γ structure are in the same plane as the PT backbone planes with "step-side" (wavy) structures. Dag and Wang[33] reported energy barriers calculated by changing the torsion angle around bond connection between PT backbone and the side chain for an isolated single rr-P3HT chain, and two local minima at 0° and 85° were found; the angle at 0° is slightly favorable than 85° with the energy difference of 0.1 eV. The other is the interplanar offset δ_b as listed in Table II; type β has $\delta_b = b/2$, but type γ exhibits $\delta_b = b/5$ [see Figs. 4(b) and 5(b)].

As a result of full structural relaxation performed for type γ using the pseudopotential method, we found lattice parameters, $a = 16.27$ Å, $b = 7.72$ Å, $c = 7.15$ Å, and $\beta = 89.02^\circ$, as presented in Fig. 4(c) and 4(d) (called type γ'). From type γ to γ', their optimized lattice parameters are consistent with experimentally determined structures, but the lattice constant c (the PT backbone stacking direction) is shorter than that of the experimentally determined lattice constant. The corresponding interplanar distance is decreased from 3.6 to 3.1 Å, and their internal atomic coordinates are drastically changed, as shown in Fig. 5. After the relaxation, the step-side structure is gone; the molecular sheets have been straightened in the ab plane. This optimized structure is very similar to the schematic model proposed by Tashiro *et al.*[22] The offset δ_b is significantly decreased ($\delta_b = 0.058b$) as shown in Fig. 5(d). In the experimental structure, the tails of the hexyl side chain are very close to that of the neighboring chain, as shown in Fig. 5(a) and 5(b). Thus, it can be interpreted that the molecular sheet has been moved in order to secure space for the hexyl side chain in the unit cell. In the optimized structure, the side chains have enough space to stretch their tails and are interjected with tails of neighboring side chains [see Fig. 5(c) and 5(d)]. However, we found that the γ' structure is less stable than the β' structure; the total energy difference is 1.32 eV per 50 atoms, as listed in Table III.

Recently Xie *et al.* have also performed the full structural relaxations for the experimentally determined structure.[35] Their relaxed structure is slightly different from γ' structure in the present study. Their result also shows that the step-side (wavy) structure disappears due to the cell relaxation. However, the offset δ_b has not changed from the experimental structure, and the lattice constant a has a longer value of 18.91 Å than the experimental one of 16.0 Å and type γ' of 16.27 Å. No interdigitation of the side chains is found in the structure. Although vdW interactions are partially included in their relaxation, their lattice constant c of 6.63 Å, which along the π-stacking direction is shorter than our LDA result of 7.15 Å and the experimental one of 7.8 Å. It was reported that the relaxed monoclinic structure is energetically unfavorable, and the most stable structure in their study is an orthorhombic structure with $a = 17.24$ Å, $b = 7.80$ Å, $c = 7.70$ Å. Additionally, the offset $\delta_b = 0$ is stabilized at $\beta = 90^\circ$ in the orthorhombic structure on the basis of the DFT + LAP calculations.

3. *Monoclinic structure with $P2_1$*

Motivated by the orthorhombic structure, we tried to find more stable structure than the β' structure. We assumed a structure with space group $P2_1$ (No. 4) to have no slippage between the upper and lower sheet ($\delta_b = 0$) as shown in Fig. 6. The lattice contains only a single layer with 50 atoms, and the lattice constant c has almost half that of the other structures. The original internal coordinates are based on an experimental structure by Kayunkid *et al.* We term this structure type κ. We performed the full lattice relaxations for the structure by using the VASP code within LDA. The relaxed lattice parameters are $a = 18.56$ Å, $b = 7.74$ Å, $c = 3.74$ Å, and $\beta = 86.57^\circ$ (type κ'). The LDA results clearly show that the monoclinic angle is not stabilized by the offset $\delta_b = 0$. The lattice constant a is longer than that of other structures as listed in Table II, and no interdigitations of side chains are observed (see Fig. 6). As listed in Table III, the κ' structure is more stable than γ', but

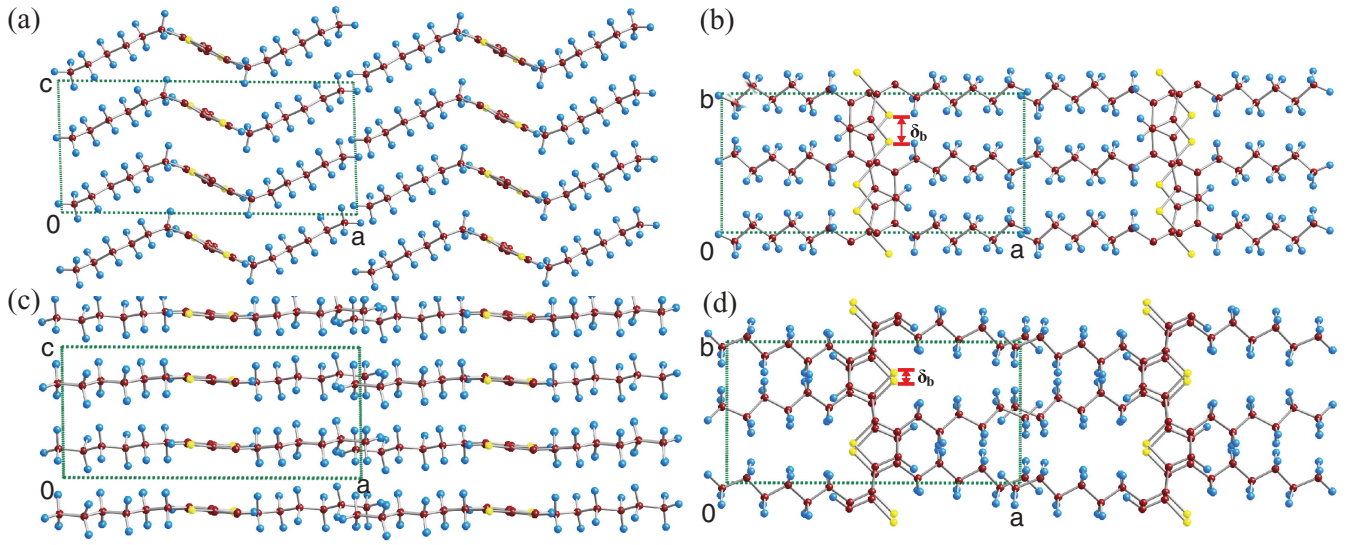

FIG. 5. (Color online) Crystal structure of type γ and γ'. (a) Longitudinal views of γ structure along the b axis showing the ac plane. (b) Orthogonal views of γ structure along the c axis showing the ab plane. (c) Longitudinal views of γ' structure along the b axis showing the ac plane. (d) Orthogonal views of γ' structure along the c axis showing the ab plane. Yellow circles show sulfur atoms, red circles show carbon atoms, and blue circles show hydrogen atoms. Green dashed lines represent a conventional unit cell.

less stable than the β' structure with the energy difference of 0.37 eV/50 atoms. Indirect and direct band gaps of 0.75 and 1.01 eV are found, respectively, in the κ' structure.

In this study we found that the β' structure has the lowest energy within the LDA calculations (see Table III). However, the large discrepancies of the angle β and interplaner distance between PT backbones with experiment still need to be investigated. The structural stability might be determined by not only interactions between stacked PT backbones but also the configurations of the side chains. Other structures are possible to be more stable than the β' structure by introducing a better description of vdW interactions with the DFT. Implementations of DFT including the semiempirical dispersion correction[55] and vdW-DFT framework[56] are now in progress to be compared with the LDA results. Now that the molecular packing has been determined, we can discuss their linear optical properties and electronic structures.

B. Linear optical properties and electronic structure

Dielectric functions and optical transition rates are calculated for discussing their linear optical properties using the FLAPW method.[46,47] We focused on the frequency dependence of the imaginary part ε_2 of the dielectric functions, which can be derived according to Eq. (1), as plotted in Fig. 7(a) and 7(b), respectively. The optical absorption spectra calculated by Eq. (2) are shown in Fig. 8. The dielectric

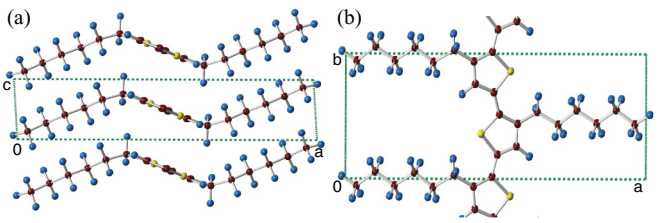

FIG. 6. (Color online) Crystal structure of type κ'. (a) Orthogonal view along the b axis showing the ac plane and (b) longitudinal view along the c axis showing the ab plane. Yellow circles show sulfur atoms, red circles show carbon atoms, and sky blue circles show hydrogen atoms. Green dashed lines represent a conventional unit cell.

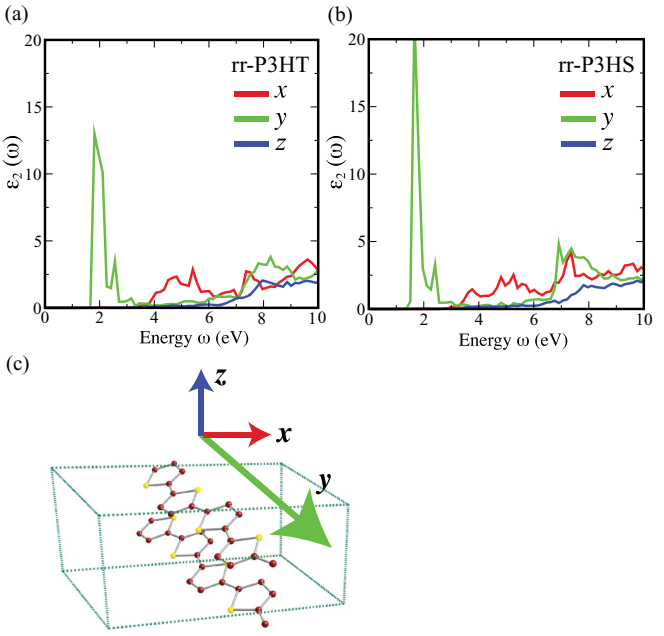

FIG. 7. (Color online) Frequency dependence of the imaginary part of dielectric functions for (a) rr-P3HT and (b) rr-P3HS with type β'. (c) Crystal structure of type β' without hexyl side chains. Yellow circles show sulfur atoms, red circles show carbon atoms. The arrows exhibit Cartesian axes, which correspond to the three components of the optical transitions.

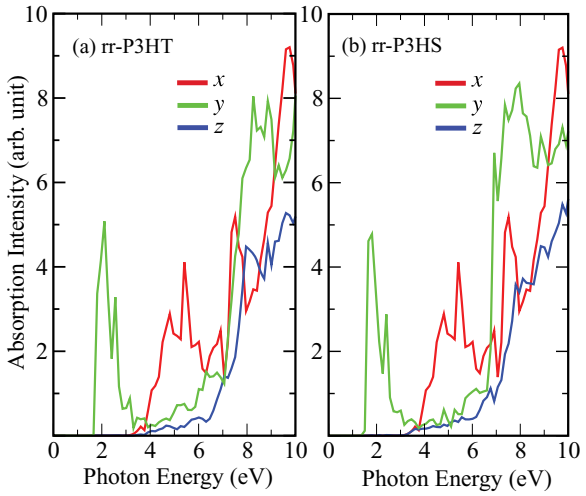

FIG. 8. (Color online) Optical absorption spectra of (a) rr-P3HT and (b) rr-P3HS. Red curves shows x, green one shows y, and blue one shows z components.

functions are calculated using the most stable structure, type β'. A scissors correction is used in the spectra, $\delta_b = 0.8$ eV, for both crystals.[57] As shown in the imaginary part of the dielectric functions, we found that the optical transition along the y axis is dominant at the band edges. The electronic band structure of β' structure is plotted in Fig. 9. The band structure was investigated by evaluating the band dispersion along k points of high symmetry in the first Brillouin zone of the monoclinic lattice. The direct band gap at Γ within the LDA is 1.01 eV, and the gap is almost constant along to the Z point, but a similar size of band gap can be seen along the Λ to M point. In this compound, the valence band maximum (VBM) is located at Γ, and the conduction band minimum (CBM) is located at the M point. There is a quite small indirect band gap of 0.1 eV between them. The high symmetry line in the Brillouin zone along Γ–Z and Λ–M corresponds to the x axis of the lattice vector. Their calculated direct band gap corresponds to the measured value of 1.8 eV found based on the absorption coefficient.[14] As expected, these LDA results underestimate the value of the band gap. Hence, we are performing screened exchange calculations to obtain more reliable band gaps.

The calculated contour plots of wave functions at the VBM and CBM at the Λ and Γ points are also shown in Figs. 9(a)–9(d). Here, the most interesting point is that only the C and S orbitals belonging to polythiophene backbones can be seen in these plots, and there is no contribution from the hexyl side chains. Total and partial DOS of β' structures are also shown in Fig. 9. In the crystal structure, there are 10 atomic (Wycoff) sites of C atoms in the unit cell, which can be classified into two groups: one belonging to polythiophene backbones, and the other is a part of the hexyl side chain. The band structure and the partial DOS with the classification are plotted in Fig. 9. We found that the well-bent bands at occupied states between–4 and 0 eV, and the unoccupied states are made of mostly p_π orbitals of C and S atoms, but the flat bands below–4 eV composed of C and H orbitals belong to the hexyl side chains. Almost all C bondings in the hexyl side chains are made of only σ bonds, with none from π bonding at all in this energy region.

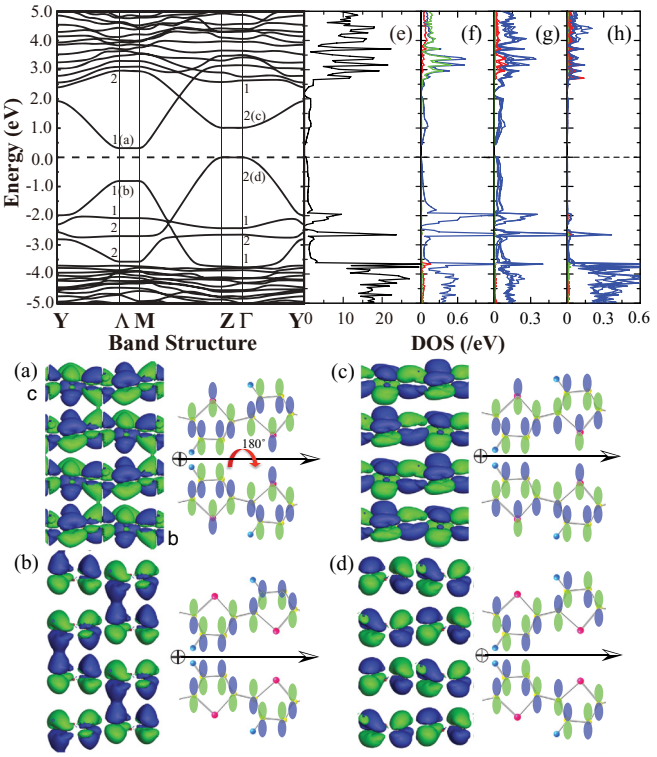

FIG. 9. (Color online) Energy band structure and total and partial DOS of type β', a base-centered monoclinic structure ($A2$) with lattice parameters $a = 16.23$ Å, $b = 7.73$ Å, $c = 7.03$ Å, and $\beta = 101.24°$. The x axis represents k points of high symmetry in the first Brillouin zone of the base-centered monoclinic lattice, labeled as $Y(0, 0, 0.5)$, $\Lambda(0, 0.5, 0.5)$, $M(0.5, 0.5, 0.5)$, $Z(0.5, 0, 0)$, and $\Gamma(0, 0, 0)$ in terms of the reciprocal unit vectors. The origin of the y axis is set to be at the valence band maximum. Numbers written in each band show an irreducible representation of wave functions of each state at Λ and Γ (Γ_x, $x = 1$ or 2) Corresponding contour plots of wave functions at (a) CBM and (b) VBM at the Λ point and (c) CBM and (d) VBM at the Γ point. (e) Total and partial DOS of (f) S-s (red), p (blue), d (green) orbitals, and C-s and p orbitals belonging to (g) the backbones and (h) side chains.

1. Matrix elements

To better understand how the intrinsic electronic structure affects the optical transitions of the polymers, it is useful to evaluate the electric dipole matrix elements from a group-theoretical view.[48,58–60] The matrix element includes all symmetry issues; an electric dipole transition can be forbidden by the symmetry of the molecule or crystal, which is called the dipole selection rule. The electric dipole operator $\mathbf{p}$ is a vector which has three components, p_x, p_y, and p_z, and is an odd function; the operator has the same symmetry as a polar vector $\hat{\mathbf{e}}$. Whether an optical transition is forbidden or not can be ascertained by examining the direct product of the symmetries of initial and final states in the vertical optical transition.[58] In β' structure, all atomic coordinates occupied in the $2a$ site of the space group belong to the point group C_2. The corresponding character table is shown in Table IV. The matrix element is nonzero if $\Gamma^{(f)}$ is contained in the decomposition of the direct product between the dipole operator $\mathbf{p}$ and an irreducible representation of initial state $\Gamma^{(i)}$. Since $\mathbf{p}$ is transformed by the representation at $\mathbf{k} = 0$; $\Gamma_{\mathbf{p}} = \Gamma_2^-$ irreducible representation in

TABLE IV. Character table of irreducible representation of the C_2 point groups.

C_2	E	2	
$\Gamma_1(A_g)$	1	1	x, z, R_y
$\Gamma_2(A_u)$	1	−1	y, R_x, R_z

the group C_2, We are concerned with a vertical transition from the top of the valence bands at the Γ point; the direct product transforms as

$$\Gamma_{\mathbf{p}} \times \Gamma^{(i)} = \Gamma_2^- \times \Gamma_2^- = \Gamma_2^- + \Gamma_1^+. \quad (3)$$

Since Γ_2^- and Γ_1^+ are contained, the dipole transitions into all levels are allowed. At the Λ point, the direct product is given by

$$\Gamma_{\mathbf{p}} \times \Lambda^{(i)} = \Gamma_2^- \times \Lambda_1^+ = \Lambda_2^- + \Lambda_1^+; \quad (4)$$

the transitions into all levels are also allowed.

As shown in Fig. 7, at the top of the valence band Γ and Λ, only the yy component remains in the matrix elements. Both band edges have a significant contribution from the backbone, but almost none from the alkyl side chains. For instance, the top of the valence band at Γ is set to be an initial state; an irreducible representation of the initial wave function ψ_i belongs to the Γ_2 irreducible representation. The bottom of the conduction band is set to be the final state, which also belongs to the representation

$$Rp_x = p_x^-, \quad Rp_y = p_y^+, \quad Rp_z = p_z^-. \quad (5)$$

Here R represents the space group symmetry operation. As shown in Fig. 9, the upper and lower molecular sheet in the unit cell are connected by a rotation symmetry of 180° around the y axis. Using the character table, we can apply the operation of the symmetry R for the initial and final state wave functions ψ at the Γ point:

$$R\psi_f = \psi_f^-, \quad R\psi_i = \psi_i^-. \quad (6)$$

The sign of the x and z components of wave functions is changed by the asymmetric operations, but the component y is invariant under every operation of this group. The matrix elements can be written as $\langle\psi_f|p_i|\psi_i\rangle = R\langle\psi_f|p_i|\psi_i\rangle$. For $i = y$, $\langle\psi_f^-|p_i^+|\psi_i^-\rangle$ is nonzero. For $i = x$ and z, $\langle\psi_f^-|p_i^-|\psi_i^-\rangle$ vanished. At the Λ point, wave functions at the top of the valence and bottom of the conduction bands belong to symmetric representations:

$$R\psi_f = \psi_f^+, \quad R\psi_i = \psi_i^+. \quad (7)$$

The matrix element for the y component is $\langle\psi_f^+|p_i^+|\psi_i^+\rangle$, and that for x and z is written as $\langle\psi_f^+|p_i^-|\psi_i^+\rangle$. Thus, the transitions with x and z polarized light are forbidden at both band edges within the dipole approximation.

As a result of an analysis of the character of the wave functions at the band edges and partial density of states, the d band tails of S atoms and the p component of C are dominant at the top of the valence bands. There are fewer S-p orbitals, but a large amplitude of the p orbital can be seen at the bottom of the conduction band. These S orbitals are hybridized with p orbitals of C atoms belonging to the PT backbones. These C-p orbitals have an on-site hybridization of their d orbitals.

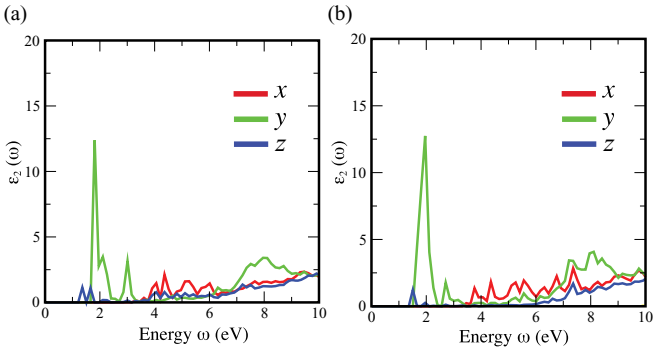

FIG. 10. (Color online) Frequency dependence of the imaginary part of dielectric functions for rr-P3HT with (a) type γ and (b) type γ'. The arrows exhibit Cartesian axes, which correspond to the three components of the optical transitions.

The electric dipole transitions from s to p, and from p to d orbitals of Se/S and C are allowed.

In this study imaginary part of dielectric functions for the γ and γ' structures were also calculated as shown in Fig. 10(a) and 10(b). In both spectra there are small peaks of ϵ_{zz} at the band edge, but large peaks of ϵ_{yy} are dominant. All atoms in the unit cell are belonging to the C_{2v} point group. This group has C_2 operation with two mirrors σ_v(xy) and σ_v(yz). Similar explanations as type β' are available for these structures.

2. *Differences between rr-P3HT and rr-P3HS*

The differences in the structural, optical, and electronic properties between polythiophenes and polyselenophenes are studied by focusing on the effect of Se replacement in rr-P3HT.

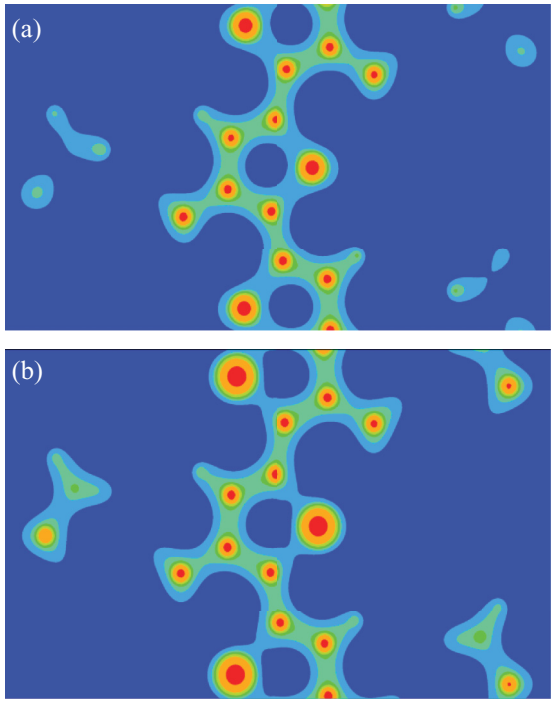

FIG. 11. (Color online) Total charge density plots of (a) rr-P3HT and (b) rr-P3HS backbone planes.

The structural optimization was performed for the most stable structure, type β', with substitution of sulfur by selenium. The relaxed structural parameters of rr-P3HS are $a = 15.87$Å, $b = 7.98$ Å, $c = 7.13$ Å, and $\beta = 100.35^\circ$. There is no big difference between them, the lattice constant b of P3HS is slightly larger than P3HT, which might come from the difference in ionic radius between S and Se, as shown in the total charge density maps of Fig. 11. The overlap of the charge density between C and S (Se) is not significant. The electronic structure of rr-P3HS can be considered as a semiconductor with a direct band gap of 0.86 eV within LDA as listed in Table III. The direct band gap of P3HS is 20% smaller than that of P3HT, and this ratio is in fairly good agreement with measurements; the band width of P3HS is decreasing. The p orbitals of Se are higher in energy compared to that of P3HT; the p orbitals of Se are more delocalized (extended in space) than those of S atoms. The band width of P3HS is smaller, and Se orbitals are at a higher energy compared to those of P3HT. As shown in Fig. 7, the peak of imaginary part of the dielectric function ϵ_2 of rr-P3HS is higher than that of rr-P3HT at below 4 eV, but the absorption spectra μ of rr-P3HS are almost identical to that of rr-P3HT (see Fig. 8).

C. Summary

Using first-principles DFT calculation methods, linear optical properties, electronic structure, and the structural stabilities of rr-P3HT and rr-P3HS were investigated by focusing on their anisotropic structure. Several possible crystal structures are proposed, and their structural stabilities are discussed by performing structural optimizations within the LDA. The most stable structure is a base-centered monoclinic structure (type β'), belong to the $A2$ space group with the lattice parameters of $a = 16.23$ Å, $b = 7.73$ Å, $c = 7.03$ Å, and $\beta = 101.24^\circ$. The optical spectra are evaluated by calculating its dielectric functions, focusing on the frequency dependence of the imaginary part, and a group-theoretical analysis of the matrix elements is given to explain the interband transitions. Strong y-polarized optical absorption is found at below 4 eV, which is associated with the π conjugation of the PT backbones. It is also found that extended p orbitals of C and S atoms belonging to the PT backbones have a significant contribution at the VBM and CBM, but there is almost no contribution from the hexyl side chains to the optical transitions. The differences in electronic and optical properties between rr-P3HT and rr-P3HS are discussed; the calculated direct band gap within LDA of P3HS, 0.86 eV, is about 20% smaller than that of rr-P3HT, 1.10 eV, but the band gap difference does not significantly affect the optical absorption coefficients.

ACKNOWLEDGMENTS

Work was supported by the Argonne-Northwestern Solar Energy Research (ANSER) Center, an Energy Frontier Research Center funded by the US Department of Energy, Office of Science, Office of Basic Energy Sciences under Award Number DE-SC0001059 and DE-FG02-06ER46320.

*Present address: RIKEN, Wako, Saitama 351-0198, Japan; tsumu@riken.jp

†Jung-Hwan Song is deceased.

[1] G. Yu, J. Gao, J. C. Hummelen, F. Wudl, and A. J. Heeger, Science **270**, 1789 (1995).

[2] G. Li, V. Shrotriya, J. Huang, Y. Yao, T. Moriarty, K. Emery, and Y. Yang, Nat. Mater. **4**, 864 (2005).

[3] A. C. Mayer, S. R. Scully, B. E. Hardin, M. W. Rowell, and M. D. McGehee, Mater. Today **10**, 28 (2007).

[4] A. Patra and M. Bendikov, J. Mater. Chem. **20**, 422 (2010).

[5] H. Sirringhaus, P. J. Brown, R. H. Friend, M. M. Nielsen, K. Bechgaard, B. M. W. Langeveld-Voss, A. J. H. Spiering, R. A. J. Janssen, E. W. Meijer, P. Herwig, and D. M. de Leeuw, Nature (London) **401**, 685 (1999).

[6] G. Wang, J. Swensen, D. Moses, and A. J. Heeger, J. Appl. Phys. **93**, 6137 (2003).

[7] A. S. Dhoot, G. M. Wang, D. Moses, and A. J. Heeger, Phys. Rev. Lett. **96**, 246403 (2006).

[8] A. Salleo, Mater. Today **10**, 38 (2007).

[9] S. R. Forrest, Nature (London) **428**, 911 (2004).

[10] M. T. Rispens, A. Meetsma, R. Rittberger, C. J. Brabec, N. S. Sariciftci, and J. C. Hummelen, Chem. Commun. No. **17**, 2116 (2003).

[11] V. Chu, J. Jarego, H. Silva, T. Silva, M. Reissner, P. Brogueira, and J. P. Conde, Appl. Phys. Lett. **70**, 2714 (1997).

[12] J. C. Guo, Y. Y. Liang, Y. Szarko, B. Lee, H. J. Son, B. S. Rolczynski, L. P. Yu, and L. X. Chen, J. Phys. Chem. B **114**, 742 (2010).

[13] J. M. Szarko, J. Guo, Y. Liang, B. Lee, B. S. Rolczynski, J. Strzalka, T. Xu, S. Loser, T. J. Marks, L. Yu, and L. X. Chen, Adv. Mater. **22**, 5468 (2010).

[14] A.-T. Chen, X. Wu, and R. D. Rinke, J. Am. Chem. Soc. **117**, 233 (1995).

[15] R. Österbacka, C. P. An, X. M. Jiang, and Z. V. Vardeny, Science **287**, 839 (2000).

[16] S. Ukai, H. Ito, K. Marumoto, and S. Kuroda, J. Phys. Soc. Jpn. **74**, 3314 (2005).

[17] E. J. Samuelsen, and J. Mørdalen, *Handbook of Organic Conductive Moleculars and Polymers, Vol. 3* (John Wiley and Sons, New York, 1997), p. 87.

[18] T. J. Prosa, M. J. Winokur, and R. D. MuCullough, Macromolecules **29**, 3654 (1996).

[19] A. Buono, N. H. Son, G. Raos, L. Gila, A. Cominetti, M. Catellani, and S. V. Meille, Macromolecules **43**, 6772 (2010).

[20] M. Brinkmann, J. Polym. Sci., Part B: Polym. Lett. **49**, 1218 (2011).

[21] K. Tashiro, Y. Minagawa, M. Kobayashi, S. Morita, T. Kawai, and K. Yoshino, Jpn. J. Appl. Phys. **33**, L 1023 (1994).

[22] K. Tashiro, M. Kobayashi, T. Kawai, and K. Yoshino, Polymer **12**, 2867 (1997).

[23] D. Kim, J. Han, Y. Park, Y. Jang, J. Cho, M. Hwang, and K. Cho, Adv. Mater. **18**, 719 (2006).

[24] M. Brinkmann and P. Rannou, Adv. Funct. Mater. **17**, 101 (2007).

[25] M. Brinkmann and J. C. Wittmann, Adv. Mater. **18**, 860 (2006).

[26] R. Rannou and M. Brinkmann, Macromolecules **42**, 1125 (2009).

[27]T. J. Prosa, M. J. Winokur, J. Moulton, J. Smith, and A. J. Heeger, Macromolecules **25**, 4364 (1992).
[28]T. J. Prosa, M. J. Winokur, J. Moulton, P. Smith, and A. J. Heeger, Phys. Rev. B **51**, 159 (1995).
[29]N. Kayunkid, S. Uttiya, and M. Brinkmann, Macromolecules **43**, 4961 (2010).
[30]J. E. Northrup, Phys. Rev. B **76**, 245202 (2007).
[31]J. E. Northrup, M. L. Chabinyc, R. Hamilton, I. McCulloch, and M. Heeney, J. Appl. Phys. **104**, 083705 (2008).
[32]A. Maillard and A. Rochefort, Phys. Rev. B **79**, 115207 (2009).
[33]S. Dag and L. W. Wang, J. Phys. Chem. B **114**, 5997 (2010).
[34]R. Colle, G. Grosso, R. Ronzani, and M. Zicovich-Wilson, Phys. Status Solidi B **1**, 1 (2011).
[35]W. Xie, Y. Y. Sun, S. B. Zhang, and J. E. Northrup, Phys. Rev. B **83**, 184117 (2011).
[36]A. M. Ballantyne, L. Chen, J. Nelson, D. D. C. Bradley, Y. Astuti, A. Maurano, C. G. Shuttle, J. R. Durrant, M. Heeney, W. Duffy, and I. McCulloch, Adv. Mater. **19**, 4544 (2007).
[37]M. Heeney, W. Zhang, D. J. Crouch, M. L. Chabinyc, S. Gordeyev, R. Hamilton, S. J. Higgins, I. McCulloch, P. J. Skabara, D. Sparrowe, and S. Tierney, Chem. Commun. **47**, 5061 (2007).
[38]A. M. Ballantyne, T. A. M. Ferenczi, M. Campoy-Quiles, T. M. Clarke, A. Maurano, K. H. Wong, W. Zhang, N. Stingelin-Stutzmann, J.-S. Kim, D. D. C. Bradley, J. R. Durrant, I. McCulloch, M. Heeney, and J. Nelson, Macromolecules **43**, 1169 (2010).
[39]M. Weinert, J. Math. Phys. **22**, 2433 (1981).
[40]E. Wimmer, H. Krakauer, M. Weinert, and A. J. Freeman, Phys. Rev. B **24**, 864 (1981).
[41]O. K. Andersen, Phys. Rev. B **12**, 3060 (1975).
[42]D. D. Koellng and G. O. Arbman, J. Phys. F **5**, 2041 (1975).
[43]P. Hohenberg and W. Kohn, Phys. Rev. B **136**, 864 (1964).
[44]W. Kohn and L. J. Sham, Phys. Rev. **140**, 1133 (1965).
[45]L. Hedin and B. I. Lundqvist, J. Phys. C **4**, 2064 (1971).
[46]R. Asahi, W. Mannstadt, and A. J. Freeman, Phys. Rev. B **59**, 7486 (1999).
[47]J. Li and A. J. Freeman, Phys. Rev. B **74**, 075333 (2006).
[48]D. W. Lynch, *Interband Absorption-Mechanisms and Interpretation, Handbook of Optical Constants of Solids* (Academic Press, New York, 1985).
[49]G. Kresse and J. Hafner, Phys. Rev. B **47**, 558 (1993).
[50]G. Kresse and D. Joubert, Phys. Rev. B **59**, 1758 (1999).
[51]P. Arosio, M. Moreno, A. Famulari, G. Raos, M. Catellani, and S. V. Meille, Chem. Mater. **21**, 78 (2009).
[52]P. Arosio, A. Famulari, M. Catellani, S. Luzzati, L. Torsi, and S. V. Meille, Macromolecules **40**, 3 (2007).
[53]K. E. Aasmundtveit, E. J. Samulsen, L. A. A. Petterson, O. Omgamas, and R. Feridenhans, Synth. Met. **101**, 561 (1999).
[54]E.-G. Kim and J.-L. Bredas, J. Am. Chem. Soc. **130**, 16880 (2008).
[55]J. Antony and S. Grimme, Phys Chem Chem Phys **8**, 5287 (2006).
[56]M. Dion, H. Rydberg, E. Schröder, D. C. Langreth, and B. I. Lundqvist, Phys. Rev. Lett. **92**, 246401 (2004).
[57]F. Nastos, B. Olejnik, K. Schwarz, and J. E. Sipe, Phys. Rev. B **72**, 045223 (2005).
[58]M. Lax, *Symmetry Principles in Solid State and Molecular Physics* (John Wiley, New York, 1974).
[59]P. Y. Yu and M. Cardona, *Fundamentals of Semiconductors, Physics and Materials Properties* (Springer, Berlin, 2005).
[60]A. S. Davydov, Ukr. Phys. J. **53**, 65 (2008).
[61]T. Kawai, M. Nakazono, R. Sugimoto, and K. Yoshino, J. Phys. Soc. Jpn. **61**, 3400 (1992).